Infrared and Raman spectroscopy of the organic crystal DAST: Polarization dependence and contribution of molecular vibrations to the linear electro-optic effect

Ch. Bosshard,[1,*] R. Spreiter,[1] L. Degiorgi,[2] and P. Günter[1]

[1]*Nonlinear Optics Laboratory, Institute of Quantum Electronics, ETH Hönggerberg, CH-8093 Zürich, Switzerland*
[2]*Solid State Physics, ETH Zürich, CH-8093 Zürich, Switzerland*

We use infrared spectroscopy and Raman scattering to show that molecular vibrations considerably contribute to the linear electro-optic effect in the highly nonlinear optical organic crystal 4-N,N-dimethylamino-4$'$-N$'$-methyl stilbazolium tosylate (DAST). In addition to the almost negligible acoustic contribution (smaller than 2%), the vibrational contributions are estimated to reach 25% in DAST. Using infrared and Raman spectroscopy, as well as force-field calculations, the strongest vibrational modes contributing to the electro-optic effect are identified as in plane aromatic ring deformations and carbon-carbon stretching modes. In addition, we present experimental results on absorption coefficients and refractive indices in the infrared which have also an important impact on THz generation and detection using DAST crystals.

I. INTRODUCTION

The linear electro-optic effect allows us to control a light beam by an electric field and is therefore of prime interest for the design of the interfaces between optical and electrical communication networks. Because the electro-optic effect in organic single crystals is of mainly electronic origin, they are very attractive electro-optic materials. These materials offer almost unlimited design possibilities to fine-tune their optical properties and lead to large electro-optic effects with short response times. Among these materials, the organic salt 4-N,N-dimethylamino-4$'$-N$'$-methyl stilbazolium tosylate (DAST) is one of the most promising for electro-optic modulation[1–3] and THz generation[4,5] (Fig. 1).

Often, the linear electro-optic effect is assumed to be constant with the frequency of the applied electric field for organic materials. In this work we show the linear electro-optic effect to be frequency dependent for the case of DAST. We demonstrate significant contributions due to molecular vibrations and discuss the linear optical properties of this material in the infrared. This work is organized as follows. Section II is devoted to the theoretical description of the frequency dependence of the linear electro-optic effect. In Sec. III we discuss the lattice vibrational contributions to the linear electro-optic effect in more detail. Section IV introduces infrared and Raman spectroscopy (Sec. IV A) and describes the results obtained from infrared (Sec. IV B) and Raman (Sec. IV C) measurements of DAST. In Sec. IV D the experimental results are compared to theoretical calculations in order to identify the vibrational modes. Section IV E is devoted to a short discussion on the influence of the environment on the molecular vibrations. Finally, the conclusions of the work presented here are summarized in Sec. V.

II. FREQUENCY DEPENDENCE OF THE LINEAR ELECTRO-OPTIC EFFECT

The linear electro-optic effect is defined as the change (deformation and/or rotation) of the optical indicatrix $(1/n^2)_{ij} x_i x_j = 1$ by an applied external electric field **E**:

$$\Delta \left(\frac{1}{n^2} \right)_{ij} = r_{ijk} E_k, \qquad (1)$$

where r_{ijk} is the linear electro-optic tensor (Pockels tensor). Higher order effects are much weaker and can be neglected for practical fields ($\approx$ kV/cm). Symmetry considerations show that in the dipole approximation the quadratic effect occurs in any material, but the linear effect is present only in noncentrosymmetric materials. In the case of nonlinear optical effects, such as, e.g., optical frequency doubling, all applied and generated electric fields are oscillating with high frequencies and only the electrons are able to follow the oscillations of these fields. In this case one speaks of a purely electronic nonlinearity. In electro-optics, the situation is quite different, because the applied electric field has a much lower frequency than the optical field and, in addition to the electrons, also the atomic nuclei and even whole molecules have time to adopt a new position. This leads to two additional contributions from molecular and acoustic lattice vibrations [Eq. (2)].

In general, r_{ijk} can be written as the change of the dielectric constant with respect to the applied electric field and is given as a sum of electronic (r^e), infrared vibrational (r^o), and acoustic mode (r^a) contributions

$$r_{ijk} = \frac{-1}{n_i^2 n_j^2} \frac{d\varepsilon_{ij}}{dE_k}$$

$$= \underbrace{\frac{-1}{n_i^2 n_j^2} \frac{d\varepsilon_{ij}}{dE_k} \bigg|_{Q=u=0}}_{r_{ijk}^e} + \underbrace{\frac{-1}{n_i^2 n_j^2} \sum_n \left(\frac{d\varepsilon_{ij}}{dQ^n} \frac{dQ^n}{dE_k} \right)}_{r_{ijk}^o}$$

$$+ \underbrace{\frac{-1}{n_i^2 n_j^2} \frac{d\varepsilon_{ij}}{du_{LM}} \frac{du_{LM}}{dE_k}}_{r_{ijk}^a}, \qquad (2)$$
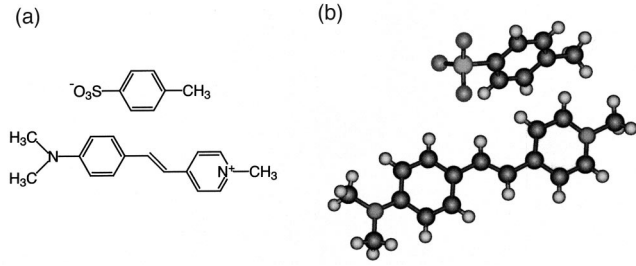
(a)

(b)

FIG. 1. Structure of the organic salt 4-N,N-dimethylamino-4'-N'-methyl stilbazolium tosylate (DAST). (a) Molecular units: The negatively charged tosylate and the positively charged, nonlinear optical chromophore stibazolium. The direction of the charge-transfer axis of the stilbazolium is defined by the two nitrogen atoms (b). The molecules are displayed as they are embedded in the crystal lattice.

where Q's are optic mode (molecular vibrational mode) displacements and u represents the elastic deformations of the crystal. The sum has to be extended over all vibrational modes of the crystal (molecular modes and lattice modes). However, only modes which are both Raman $[(d\varepsilon_{ij})/(dQ^n) \neq 0]$ as well as infrared $[(dQ^n)/(dE_k) \neq 0]$ active are contributing to the linear electro-optic effect.

The electronic contribution in Eq. (2) is given by

$$r^e_{ijk} = \frac{-1}{n_i^2 n_j^2} \frac{d\varepsilon_{ij}}{dE_k}\bigg|_{Q=u=0} \quad (3)$$

and is the electro-optic effect in absence of any optic modes, molecular vibrations, and acoustic modes. It corresponds to the electro-optic effect for frequencies of the applied field above the highest molecular modes which is above about 10 THz for organic materials. This contribution was usually discussed in terms of the quantum-mechanical two level model.[6] It can be determined from second-harmonic generation experiments through

$$r^e_{ijk} = \frac{-4}{n_i^2 n_j^2} \frac{f_i^\omega f_j^\omega f_k^o}{f_k^{2\omega'} f_i^{\omega'} f_j^{\omega'}}$$
$$\times \frac{(3\omega_{eg}^2 - \omega^2)(\omega_{eg}^2 - \omega'^2)(\omega_{eg}^2 - 4\omega'^2)}{3(\omega_{eg}^2 - \omega^2)\omega_{eg}^2}$$
$$\times d_{kij}(-2\omega',\omega',\omega'), \quad (4)$$

where $d_{kij}(-2\omega',\omega',\omega')$ is the nonlinear optical coefficient and $f_i^\omega = [(n_i^\omega)^2 + 2]/3$ is the local field correction at fre-
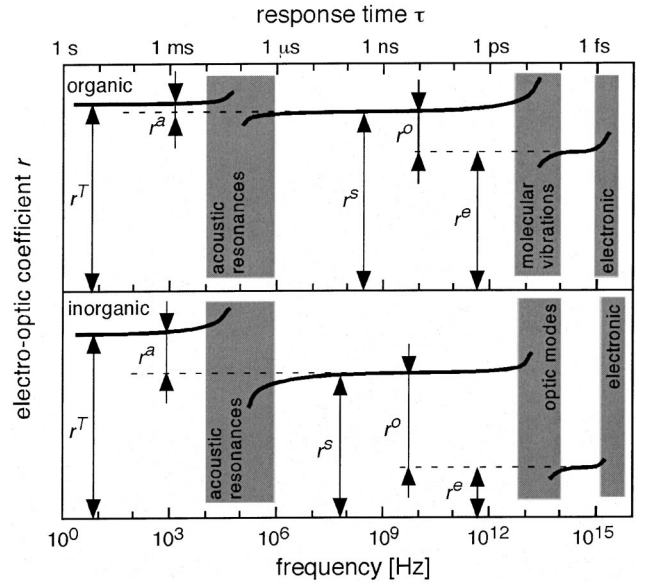

FIG. 2. Dependence of the electro-optic effect in organic (top) and inorganic (bottom) materials on the frequency of the applied field (schematically). Note that r_a can be positive or negative. In the case of r_{111} of DAST we have $r_a < 0$.

quency ω and for light polarization along i in the Lorentz approximation. Results for DAST based on Eq. (4) are given in Table I. The contribution from molecular vibrational modes is given by

$$r^o_{ijk} = \frac{-1}{n_i^2 n_j^2} \sum_n \left(\frac{d\varepsilon_{ij}}{dQ^n} \frac{dQ^n}{dE_k} \right). \quad (5)$$

Below the lowest molecular vibrational mode ($<$about 10 THz for organic materials) there exists a contribution from all the vibrational modes n being at the same time infrared active ($|dQ^n/dE_k| > 0$) and Raman active ($|d\varepsilon_{ij}/dQ^n| > 0$). This contribution will be discussed in more detail below.

The elasto-optic contribution is given by

$$r^a_{ijk} = \frac{-1}{n_i^2 n_j^2} \frac{d\varepsilon_{ij}}{du_{LM}} \frac{du_{LM}}{dE_k}. \quad (6)$$

The applied electric field may excite an elastic mode u via the converse piezoelectric effect (du_{LM}/dE_k). The elastic mode itself can produce a refractive index change via the

TABLE I. The electronic electro-optic coefficient r^e_{111}, calculated from the measured nonlinear optical coefficient d_{111} ($=290 \pm 15$ pm/V at $\lambda = 1500$ nm) (Ref. 10) and the resonance frequency $\omega_0 = 3.52 \times 10^{15}$ Hz, measured clamped and free electro-optic coefficients r^s_{111} and r_{111} and acoustic and optic phonon contributions r^a_{111} and r^o_{111} (Ref. 2).

r_{111} [pm/V] $\lambda = 1535$ nm	r^s_{111} [pm/V] $\lambda = 1535$ nm	r^e_{111} [pm/V] $\lambda = 1535$ nm	r^o_{111} [pm/V] $\lambda = 1535$ nm	r^a_{111} [pm/V] $\lambda = 1535$ nm
47 ± 8	48 ± 4	36 ± 2	12 ± 5	-1.2

elasto-optic effect ($d\varepsilon_{ij}/du_{LM}$). This contribution has been discussed in more detail for DAST in Ref. 2. These results are summarized in Table I.

To optimize a material for a large electro-optic effect with wide bandwidth, it is essential to know how the different effects contribute to the electro-optic effect at various frequencies of the applied electric field. Figure 2 shows schematically the dependence on the frequency of the applied field of the electro-optic effect in single crystals.

$r=r^T=r^e+r^o+r^a$ is the so-called free electro-optic coefficient. This is the electro-optic coefficient for frequencies lower than lowest acoustic mode of the crystal. For frequencies above the acoustic modes (MHz range), where no acoustic contributions are present, the clamped electro-optic coefficient $r^s=r^e+r^o$ is active. If the frequency is even higher than the highest optic mode frequency (100 THz range), only the electronic electro-optic contribution r^e can follow and we are in the field of nonlinear optics. In the following we will describe the infrared and Raman contributions in more detail.

III. LATTICE VIBRATIONAL CONTRIBUTIONS TO THE LINEAR ELECTRO-OPTIC EFFECT

The first-order hyperpolarizability of organic molecules is usually assumed to be of pure electronic origin (in addition to the weak contribution from acoustic phonons as discussed in the previous chapter). Only recently was it realized in this work and by *ab initio* calculations of static first-order hyperpolarizabilities[7] that nuclear relaxation may also contribute to the hyperpolarizabilities of molecules.

When an electric field is applied to a molecule, first the electron cloud is deformed. At this stage the positions of the nuclei remain the same, they are frozen in. This response is what we call a pure electronic response. In a second step, due to the changed charge distribution, the nuclei are displaced and then the nuclei and the electrons relax until equilibrium is reached. Several authors have described this second kind of contribution using different names.[7–9] Wemple *et al.*[8] and Fousek *et al.*[9] called it the ''optical phonon contribution'' wheras Del Zoppo *et al.*[7] used the ''(nuclear) relaxation contribution'' or the ''(infrared) vibrational contribution.''

Here we use an indirect method to determine the vibrational contribution to the linear electro-optic effect in DAST which is phenomenologically described by Eq. (2). In this analysis we neglect possible space-group allowed excitonic contributions. We previously investigated the high-frequency electro-optic response of DAST which allowed a determination of the acoustic and phonon contribution r^a_{111} and of r^s_{111}.[2] In addition, we calculated the electronic contribution r^e_{111} using the measured nonlinear optical coefficient d_{111}[10] and Eq. (4). The two-level equation (4) is based on was shown to be adequate for nonlinear optical coefficients of DAST.[11] By comparing the measured clamped electro-optic coefficient $r^s_{111}=r^o_{111}+r^e_{111}$ with the electronic contribution r^e_{111} we obtain $r^o_{111}=r^s_{111}-r^e_{111}=12\pm5$ pm/V. This difference of 25% can be explained by an electro-optic contribution r^o_{111} resulting from molecular vibrational modes (Table I). This conclusion relies on the accuracy of the experimental results. The nonlinear optical coefficient is determined with a
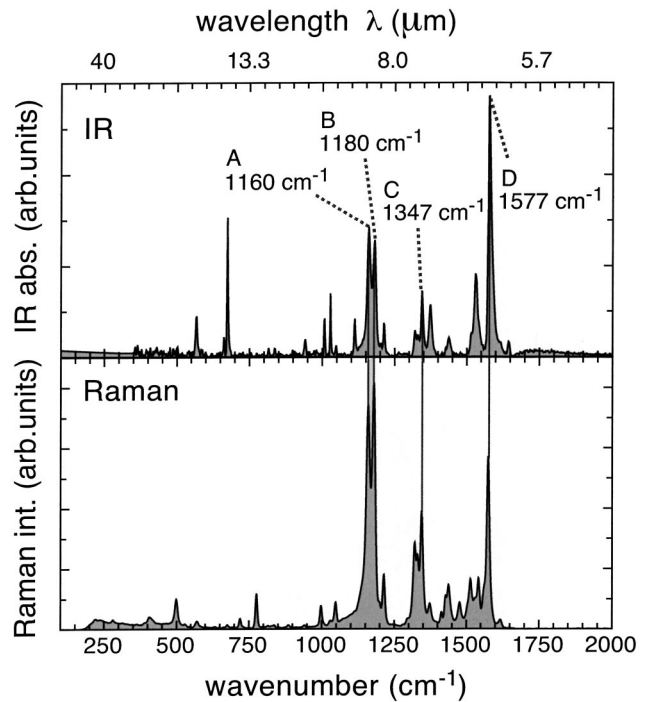

FIG. 3. Infrared (top) and Raman (bottom) spectra of crystalline DAST, both for light polarized along the polar *a* axis. Indicated are the four strongest modes which are infrared as well as Raman active.

precision of 5%.[10] This translates into the same precision for r^e_{111} using Eq. (4) since the refractive indices are known much more accurately. Combining this with the experimental 8% error of $r^s_{111}{}^2$ finally leads to the value of $r^o_{111}=12\pm5$ pm/V.

These results show that the clamped electro-optic response of DAST, and most probably also of other organic electro-optic materials, is not of pure electronic origin as it is usually assumed. There exists a considerable contribution resulting from molecular vibrational modes. Assuming the two-level model Eq. (4) to be valid, they contribute about 25% for DAST to the linear electro-optic coefficient r_{111}.

The presence of such vibrational contributions is also evident when comparing infrared spectra with Raman spectra. For contributing to the electro-optic effect, a certain vibrational mode has to be Raman and infrared active as well [see Eq. (7)]. Infrared and Raman spectra show that this is the case for the strongest modes in DAST (see Fig. 3). In the following the infrared and Raman spectra will be discussed in more detail.

It is important to note that the vibrational contributions do not affect the high frequency performance of an electro-optic material since their resonance frequencies (about 10–60 THz) are two to three orders of magnitude higher than nowaday used modulating frequencies.

IV. INFRARED AND RAMAN SPECTROSCOPY OF DAST

A. General remarks

Infrared and Raman spectroscopy are tools for the determination of the vibrational modes of molecules and crystals.

There exists only little data and knowledge about the infrared properties of organic nonlinear optical crystals, despite the fact that such measurements can provide valuable information.

(i) The refractive index and absorption coefficient in the infrared can be determined, which is important for optical parametric generators and amplifiers using organic crystals. Also for the optimization of organic materials as THz generators and detectors the far infrared dielectric properties have to be known.

(ii) Infrared and Raman spectroscopy can be used to detect the vibrational modes which, as we showed above, considerably contribute to the linear electro-optic effect in organic materials.

(iii) The vibrational frequencies depend on the crystal structure and on the force field experienced by the atoms and therefore important information on intermolecular interactions can be gained.

In a molecular crystal with N atoms per molecule and Z molecules per unit cell, each atom possesses three degrees of freedom and therefore a total of $3NZ$ vibrational modes are possible. The resulting number of modes for DAST ($N = 55$, $Z = 4$) are 3 (acoustic modes), 21 ("external" modes), and 636 ("internal" modes).[12] A complete theoretical treatment using the materials symmetries and group theory is only possible for relatively simple systems.[12] Therefore other tools for analyzing the vibrational spectra have to be applied. We will use numerical force-field calculations of the infrared modes of molecules and crystals and the comparison with tabulated literature values of characteristic group frequencies.

Both methods, Raman and infrared spectroscopy, are used to detect the vibrational modes of molecules and crystals. Since different physical effects are used in Raman and infrared spectroscopy the two methods are substantially different.

Infrared spectroscopy uses the effect of absorption of a photon having the same frequency as a vibrational mode. One photon is absorbed and generates a phonon of the same energy. To measure a spectrum the whole frequency range has to be covered by the incident radiation. All the optics (lenses, sample cell, polarizers, etc.) have to be transparent in a wide infrared wavelength range.

In Raman spectroscopy, on the other hand, the change of photon frequency due to inelastic scattering at a phonon is measured. A monochromatic incident light beam, of usually much higher frequency than any vibrational mode, is incident on the sample. A vibrational ground (Stokes) or excited (Antistokes) state of the molecule is excited to a virtual state and immediately decays into an excited (Stokes) or ground (Antistokes) vibrational state of the molecule. The frequency of the scattered photon is shifted by the frequency of the vibrational mode.

Experimentally, Raman spectroscopy is much easier than infrared spectroscopy since only one exciting wavelength is needed and the scattered light lies in a relatively narrow wavelength range in the visible or near infrared, where standard optics can be used. Also for Raman spectroscopy of solutions, infrared transparency of the solvent and sample cell is not a problem.

Not every vibrational mode is both infrared and Raman active. To be infrared active, the dipole moment μ of the molecule has to couple to the electric field of the incident radiation, whereas for Raman activity, the polarizability α has to couple to the vibrational mode. The vibrational contribution to electro-optics can be understood quite easily: The applied electric field excites the corresponding vibrational modes, i.e., results in a displacements of the nuclei. If this mode is also Raman active, the displacement modifies the polarizability of the molecule and therefore also the macroscopic refractive index.

B. Optical properties of DAST in the infrared

In order to determine the infrared modes and the dielectric properties of DAST in the infrared we used reflectometric spectroscopy. Due to the large absorption in the frequency range of vibrational modes, infrared transmission measurements are not possible for organic solid state materials.

We have measured the reflectivity spectrum $[R(\omega)]$ over a very broad frequency spectral range, extending from the far-infrared (FIR) up to the visible. We made use of four different spectrometers. The FIR spectral range was covered with a Bruker IFS 113v Fourier interferometer with a Hg arc light source and a He-cooled silicon bolometer detector. A fast scanning Bruker interferometer IFS48PC and a home-made spectrometer based on a Zeiss monochromator spectrometer were employed in the midinfrared (mid-IR) and visible spectral range, respectively. Below 5000 cm^{-1}, a gold mirror was used as reference.

The measured polarized infrared reflectance spectra was analyzed with the Kramers-Kroenig relations to calculate the refractive index and absorption. Using this approach, the real (n) and imaginary part (k) of the refractive index defined through $\tilde{n} = n + ik$ are determined by

$$n = \frac{1}{\sqrt{2}} \sqrt{\varepsilon_1 + \sqrt{\varepsilon_1^2 + \varepsilon_2^2}},$$

$$k = \frac{1}{\sqrt{2}} \sqrt{-\varepsilon_1 + \sqrt{\varepsilon_1^2 + \varepsilon_2^2}} \tag{7}$$

and the absorption coefficient α is connected to the imaginary part of the refractive index by

$$\alpha = \frac{4\pi}{\lambda} k. \tag{8}$$

The required complex dielectric constant $\hat{\varepsilon} = \varepsilon_1 + i\varepsilon_2$ can be obtained from the measured reflectance coefficient $R(\omega)$ by

$$\varepsilon_1(\omega) = \frac{[1 - R(\omega)]^2 - 4R(\omega)\sin^2\theta(\omega)}{[1 + R(\omega) - 2\sqrt{R(\omega)}\cos\theta(\omega)]^2},$$

$$\varepsilon_2(\omega) = \frac{4[1 - R(\omega)]\sqrt{R(\omega)}\sin\theta(\omega)}{[1 + R(\omega) - 2\sqrt{R(\omega)}\cos\theta(\omega)]^2}, \tag{9}$$
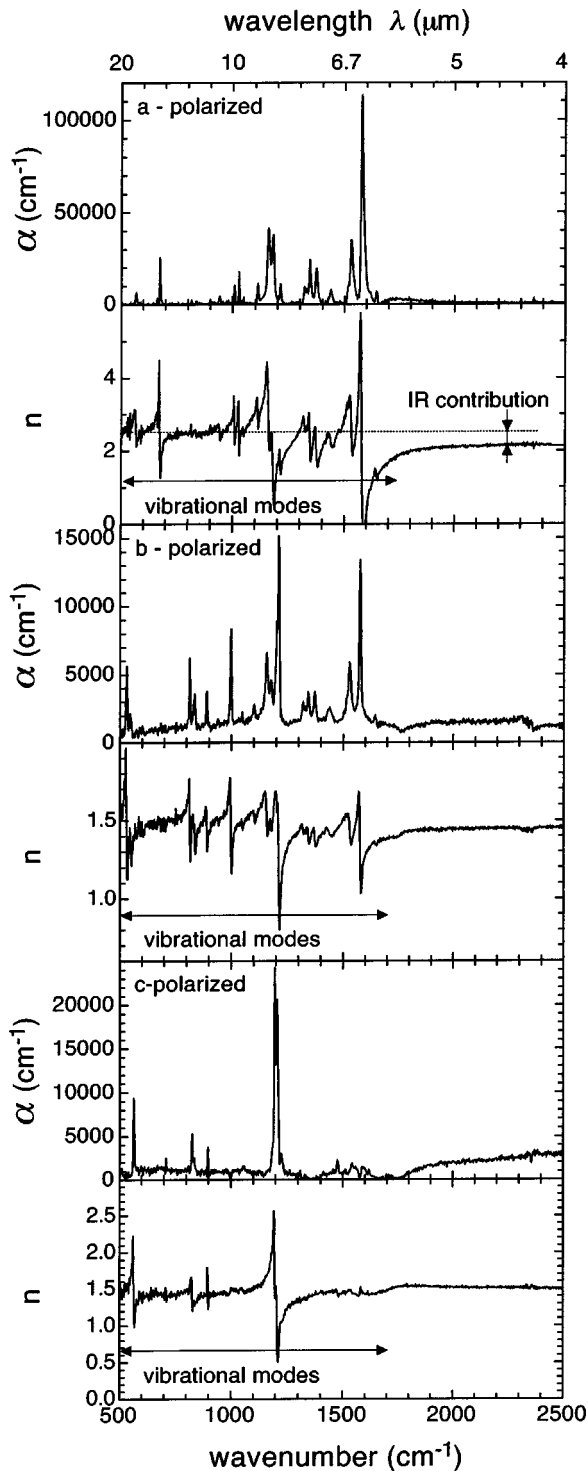
FIG. 4. Infrared absorption coefficient α and refractive index $n = \mathrm{Re}(\tilde{n})$ as calculated from the infrared reflection measurement for all three polarizations a, b, and c. The wavelength range extends from 20 down to 4 μm.

where the phase $\theta(\omega)$,

$$\theta(\omega) = \frac{\omega}{\pi} \int_0^\infty \frac{\ln\left(\frac{R(\omega')}{R(\omega)}\right)}{\omega^2 - \omega'^2} d\omega' \qquad (10)$$
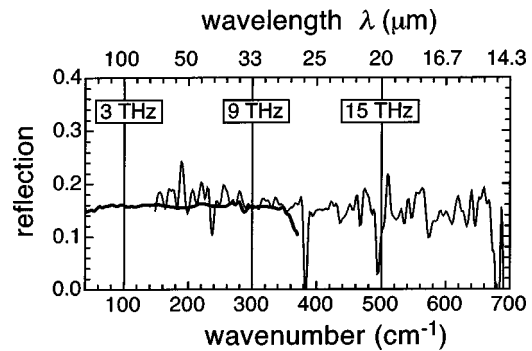

FIG. 5. Measured far infrared spectra for DAST with a polarization along the polar axis a. The two partially overlapping curves are two measurements that cover two different frequency regimes. The features of the thin solid line indicate the detection limit of the experiment and have no physical meaning.

can be calculated from the reflectance by integration over the whole frequency range.

In DAST the infrared reflectometric spectra were measured for polarizations along the a, b, and c axes of the crystal and for wave numbers from 33 000 cm^{-1} down to 50 cm^{-1} ($\lambda = 300$ nm–200 μm). Figure 4 show the absorption coefficient and the refractive index for a, b, and c polarization as calculated from the measured reflectance spectra based on the Kramers-Kroenig analysis using Eq. (9). Shown is only the frequency part where vibrational modes could be detected.

Above the resonance at about 1600 cm^{-1} a constant reflectance up to the electronic resonance was measured for all polarizations. It is important to note that the sensitivity for the absorption is very low, i.e., $k = \mathrm{Im}(\tilde{n}) = 1$ already corresponds to $\alpha = 12\,000$ cm^{-1} at $\lambda = 10$ μm. This has the effect that only the strongest resonances can be detected with this kind of measurement. The relatively weak C-H stretching modes which are expected around 3000 cm^{-1}, are completely invisible by infrared reflectometric measurements.

Although no molecular vibrational modes but only lattice modes can be expected below a wave number of about 400 cm^{-1}, the far infrared spectra in DAST down to 50 cm^{-1} (up to 200 μm) were measured. Figure 5 shows the measured reflectivity for a-polarized light, together with the lower end of the infrared measurement in Fig. 4 for comparison.

As in the case of a-polarized light (Fig. 5), a constant reflection coefficient is also measured for b and c polarization in the range from 400 to 50 cm^{-1} (25–200 μm, i.e., 12–1.5 THz). It follows that according to the Kramers-Kroenig relations, a small dispersion of the refractive indices and absorption can be expected in this frequency range. This property of DAST (and probably most organic crystals) will be of importance for the future use of DAST as a THz radiation generator and detector. The lattice modes or external modes, if present, are either too weak to be detected by this measurement or their frequency is below 50 cm^{-1}.

Such a resonance could be observed in THz transmission experiments which are more sensitive to smaller absorption coefficients. Such experiments performed in thin crystals of DAST revealed a resonance for light polarized along the a

TABLE II. Infrared contributions to the refractive index in DAST.

axis	n $\lambda = 2\ \mu m$	n $20\ \mu m < \lambda < 200\ \mu m$	vibrational IR contribution Δn_i
a	2.11	2.6 ± 0.1	0.5 ± 0.1
b	1.59	1.6 ± 0.1	< 0.05
c	1.57	1.6 ± 0.1	< 0.05

axis near 1.1 THz ($\cong 37\ \mathrm{cm}^{-1} \cong 270\ \mu\mathrm{m}$).[13] This resonance is outside the frequency range of our reflection experiments (Fig. 5). The maximum absorption coefficient obtained in that work was $\alpha_1 \approx 250\ \mathrm{cm}^{-1}$ which corresponds to an imaginary part of the refractive index of $k \approx 0.6$. Why the refractive index determined between 0.2 and 3 THz ($n_1 \approx 2.3$ at 3 THz) differs from our values ($n_1 = 2.6 \pm 0.1$) is not clear at the moment.

By comparing the refractive index above ($> 2000\ \mathrm{cm}^{-1}$) and below ($< 500\ \mathrm{cm}^{-1}$) the dominant resonances, we obtain the contribution of the molecular vibrational modes to the refractive index in the far infrared. In Table II the refractive indices at a wavelength of $\lambda = 2\ \mu\mathrm{m}$, taken from refractive index measurement,[1] the measured vibrational far infrared contribution, and the estimated refractive index in the far infrared calculated from the former values are given for DAST.

For polarization along the polar a axis there is a large contribution of molecular vibrational modes to the refractive index in the far infrared ($\lambda > 20\ \mu\mathrm{m}$) of $\Delta n_1 = 0.5 \pm 0.1$. For polarizations along the b and c axes the vibrational contributions Δn_2 and Δn_3 are smaller than 0.05 which is below the detection limit of the infrared reflectometric measurement. This very different behavior for a polarization along the
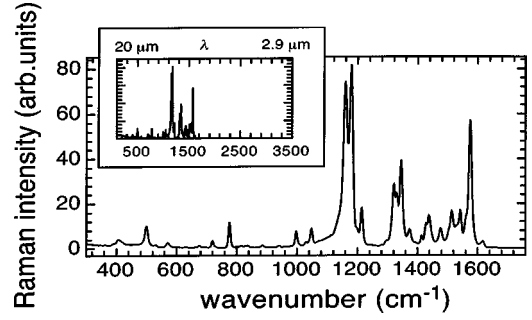

FIG. 6. Raman spectra of a DAST single crystal for light polarized along the polar a axis. The inset shows the whole frequency range which was measured. The structural features in the curves arise from the experimental set-up and not from the crystal itself.

charge transfer axis compared to the ones perpendicular to it can be well understood. It is obvious that a modification of the charge transfer axis, i.e., a vibrational mode displacing the atoms in the direction of the charge transfer axis, will result in large change of the polarizability in the same direction. In contrast, a displacement of atoms in direction where no conjugation is present will have only a small influence on the polarizability in this direction.

Since DAST belongs to the monoclinic space group Cc the optical indicatrix could rotate with wavelength and therefore, also influence the discussion above. However, no such rotations were measured between 750 and 1500 nm in DAST.[14] Moreover, rotations of the optical indicatrix in molecular crystals are often associated with bent molecules in which different parts of the molecule may show a different wavelength dispersion. In DAST the molecules are straight and no rotation of the optical indicatrix with wavelength is expected.

TABLE III. The strongest Raman lines in DAST and selected new wavelengths calculated from $\nu_m = \nu \pm m \Delta \nu$ and $\lambda = c / \nu$. (a) $\lambda = 800$ nm, (b) $\lambda = 1064$ nm, (c) $\lambda = 1300$ nm, (d) $\lambda = 1550$ nm.

| $\Delta \nu$ (cm^{-1})	λ	First Stokes ($m = -1$) (nm)	Second Stokes ($m = -2$) (nm)	First anti-Stokes ($m = 1$) (nm)	Second anti-Stokes ($m = 2$) (nm)
1160	(a)	881.8	982.3	732.1	674.8
	(b)	1213.8	1412.7	947.1	853.4
	(c)	1530.9	1861.4	1129.6	998.8
	(d)	1889.8	2420.4	1313.8	1140.0
1180	(a)	883.4	986.2	731.0	672.9
	(b)	1216.8	1420.8	945.3	850.4
	(c)	1535.6	1875.4	1127.1	994.8
	(d)	1897.0	2444.0	1310.3	1134.9
1347	(a)	898.6	1019.8	722.2	658.2
	(b)	1242.0	1491.5	930.6	827.0
	(c)	1576.0	2000.7	1106.3	962.8
	(d)	1959.0	2661.3	1282.3	1093.4
1577	(a)	915.5	1070.0	710.4	638.8
	(b)	1278.5	1601.4	911.1	796.7
	(c)	1635.2	2203.5	1078.8	922.0
	(d)	2051.4	3032.5	1245.5	1041.1
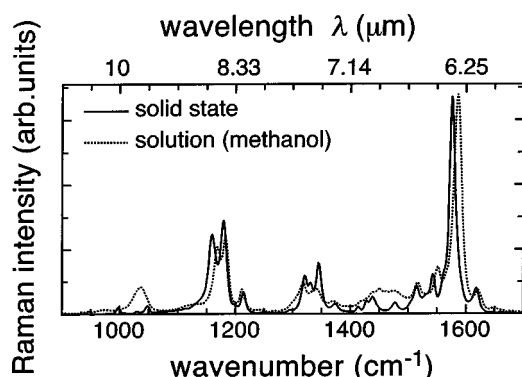
FIG. 7. Comparison of the Raman spectra of DAST in solution and in the solid state.

C. Raman spectra in solution and in the solid state of DAST

Raman scattering measurements at a fundamental wavelength of 1064 nm of DAST single crystals and DAST dissolved in methanol were performed. We used a commercial Perkin Elmer System 2000 FT IR Raman spectrometer with a fundamental pump wavelength of $\lambda = 1064$ nm (cw). For the liquid and powder samples the pump was unpolarized and no analyzer was used in front of the detection system. The light scattered perpendicular to the incident direction of the pump beam was measured by the spectrometer. For the polarized measurements a polarizer was mounted in the path of the pump beam. Note that no analyzer could be used in front of the detection system and therefore no pure Raman tensor elements could be determined.

Generally the scattered Raman intensity was very high, up to twenty times the intensity of cyclohexane, which is often used as a reference because of its high Raman activity.

Polarized Raman measurements on DAST single crystals, with incident polarizations along the a, b, and c axes were performed. For a polarization of the pump beam along the polar a axes by far the strongest Raman activity was observed with $I_a : I_b : I_c = 17 : 1.3 : 1$. The dominance from excitations along the charge transfer axis can be understood easily since a modification of the charge transfer axis of the chromophore will result in large change of the polarizability in this direction and therefore to a large Raman intensity, as we already argued for the vibrational refractive index contribution in the far infrared.

TABLE IV. Identification of the strongest infrared and Raman active modes in DAST (see Fig. 3).

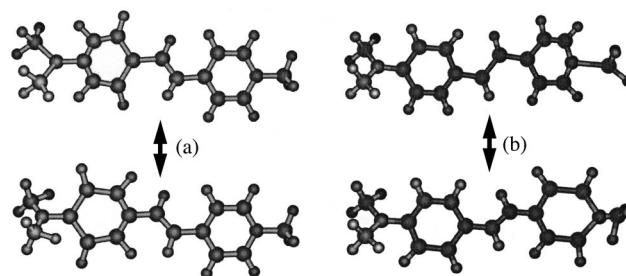| mode	wavenumber [cm^{-1}]	mode
A, B	1160	in plane aromatic ring deformations, as typi-
	1180	cal for para substituted benzenes.
C	1347	CH$_3$ umbrella deformation
D	1577	typical C-C=C-C in plane stretching frequency (carbon backbone between the aromatic rings of the stilbazolium chromophore)

FIG. 8. Calculated aromatic ring deformation modes with calculated frequencies of 1125 cm^{-1} (a) and 1280 cm^{-1} (b).

Figure 6 shows the measurement for a polarization along the polar a axis. Due to the dominance of the Raman effect along the a direction, the spectra for b- and c-polarized light show the same peaks but with much lower intensity and are not displayed here. The four strongest modes are indicated in Fig. 3. The corresponding large frequency shifts $\Delta \nu$ and selected calculated new laser wavelengths that might be generated through Raman scattering are given in Table III.

In solution (1% DAST in methanol), the same peaks as in the solid state can be identified (Fig. 7). There is a slight change in the vibrational mode frequency compared to the solid state of DAST, showing the influence of the molecular environment on the vibrational frequencies of the molecule. The strongest Raman mode for example is shifted by 9 cm^{-1} from 1586 cm^{-1} (solution) to 1577 cm^{-1} (solid state).

D. Identification of vibrational modes in DAST

In this section we will identify the strongest modes which contribute to the linear electro-optic effect in DAST. As we have seen above there is a substantial contribution to the electro-optic effect resulting from the excitation of vibrational modes. It is possible to determine the strongest modes which contribute to the electro-optic effect by comparing the Raman to the infrared vibrational spectra (Fig. 3).

The strongest contributions result from vibrational modes for which both the Raman and infrared bands are of large intensity. This is especially the case for the four modes A, B, C, and D in Fig. 3. By comparing the frequencies to correlation charts,[15] we find that the largest contributions result from aromatic ring deformations and CH$_3$ modes (Table IV).

One can easily understand that the four modes in Table IV contribute to the infrared refractive index and electro-optic effect. The aromatic ring deformations A and B are infrared
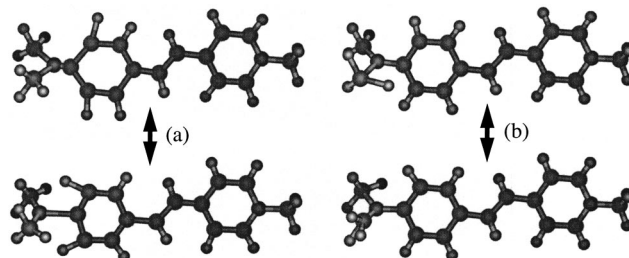

FIG. 9. Calculated C=C mode at 1552 cm^{-1} (a) and a CH$_3$ umbrella deformation mode with a calculated frequency of 1831 cm^{-1} (b).
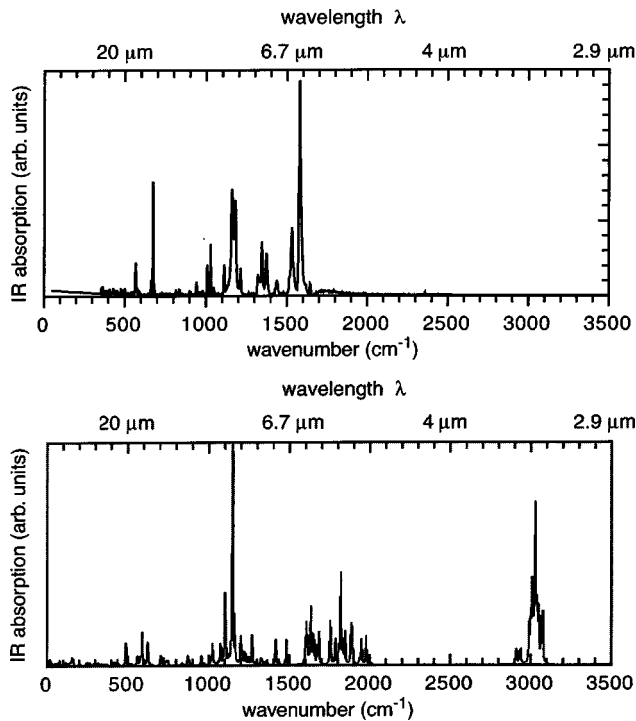
FIG. 10. Measured solid state absorption for *a*-polarized light (top) and the calculated (bottom) infrared absorption spectra.

active because of the symmetry of the molecule. Furthermore, such a deformation changes the bond length between the carbon atoms which build the charge transfer axis. The polarizability (and therefore the refractive index of the macroscopic material) of such π-conjugated charge transfer molecules is known to be strongly influenced by such changes. The same argument can be made for mode D. The influence of the CH_3 umbrella vibration can be understood since the in-phase displacement of the three H atoms changes the electronic environment for the donor and acceptor of the stilbazolium chromophore and therefore also the polarizability is modified. Also many asymmetric CH_3 modes in the range 1400–1500 cm^{-1} exist, however, with no or much smaller contribution to the optical properties.

For comparison with the measurements and to identify the most important modes, calculations of the mode frequencies and intensities were also performed. We first calculated all the vibrational modes of a molecule in the gas phase using the software CERIUS2 (Ref. 16) and the Dreiding force field parametrization.[17] The used force field parameters (spring constants) were determined experimentally using a large number of organic compounds. The eigenfrequencies are then calculated by the classical mechanical oscillator model, in which the atoms are connected by springs. The calculated modes corresponding best to the modes identified by correlation charts[15] in Table IV are visualized in Figs. 8 and 9.

E. Comparison between the calculated and measured infrared spectra of DAST

In this section we will discuss the influence of the environment on the chromophores vibrational modes. In Fig. 10 the measured infrared spectrum is compared to the calculated

one. The infrared spectrum of an infinitely extended DAST crystal (periodic boundary conditions), and not only for an isolated molecule as before, was calculated. First, the structure was optimized to the absolute energetic minima according to the Dreiding force field and then the normal modes of the whole structure are calculated.

The characteristic frequencies of the out of plane ring bending modes (500–700 cm^{-1}) and also the in plane ring deformation modes at 1100–1200 cm^{-1} are well reflected by the calculation. However, a strong deviation occurs for the symmetric and asymmetric methyl modes (1300–1500 cm^{-1}) and for the C-H stretching modes around 3000 cm^{-1}. The frequencies for the methyl modes are located about 300 cm^{-1} too high in the calculation, whereas the frequencies for the C-H stretching modes ($\approx$3000 cm^{-1}) are calculated correctly (compared to literature values[15]) but much too strong in intensity. In the measured reflection spectra they are even below the noise limit of the measurement. These observations illustrate the limitations of the calculations that do not take into account intermolecular interactions. The described discrepancy does not, however, influence the main conclusions of this paper.

V. CONCLUSION

The understanding of the underlying physical effects leading to the electro-optic response is important for the development of future materials. Three effects, with very different response times, may contribute to the linear electro-optic effect and were analyzed for the highly nonlinear optical crystal DAST.

The electronic contribution, resulting from electronic excitations, was calculated using the two level model and the nonlinear optical susceptibilities determined by optical frequency doubling.

The overall acoustic contribution to the linear electro-optic effect results from elasto-optic refractive index changes, induced by piezoelectric excitations of the crystal. The acoustic contribution in DAST was previously determined by applying a step voltage and measuring the response in the time domain.[2] The acoustic mode contribution is smaller than 2% of the overall electro-optic effect.

Up to now it was assumed that the electro-optic effect in organic materials is, in addition to a very small acoustic contribution, of almost pure electronic origin. For the first time to our knowledge, we could show that also molecular vibrational modes considerably contribute to the linear electro-optic effect in DAST. We obtained an electronic contribution of only 75% for DAST. This finding is based on the two-level model experimentally verified to be adequate for the (electronic) nonlinear optical coefficients of DAST.[11] The 25% difference could be attributed to a linear electro-optic effect resulting from vibrational infrared modes of the molecules. We confirmed the existence of such infrared and Raman active molecular vibrational modes using the measured infrared and Raman spectra as well as force field calculations and tabulated group frequencies.

INFRARED AND RAMAN SPECTROSCOPY OF THE . . .

*Present address: CSEM Alpnach, Untere Gründlistrasse 1, CH-6055 Alpnach Dorf, Switzerland. Email address: christian.bosshard@csem.ch

[1] F. Pan, G. Knöpfle, Ch. Bosshard, S. Follonier, R. Spreiter, M. S. Wong, and P. Günter, Appl. Phys. Lett. **69**, 13 (1996).

[2] R. Spreiter, Ch. Bosshard, and P. Günter, Opt. Lett. **22**, 564 (1997).

[3] F. Pan, K. McCallion, and M. Chiappetta, Appl. Phys. Lett. **74**, 492 (1999).

[4] X.-C. Zhang, X. F. Ma, Y. Jin, T.-M. Lu, E. P. Boden, P. D. Phelps, K. R. Stewart, and C. P. Yakymyshyn, Appl. Phys. Lett. **61**, 3080 (1992).

[5] P. Y. Han, M. Tani, F. Pan, and X.-C. Zhang, Opt. Lett. **25**, 675 (2000).

[6] J. L. Oudar and D. S. Chemla, J. Chem. Phys. **66**, 2664 (1977).

[7] M. Del Zoppo, C. Castiglioni, and G. Zerbi, Nonlinear Opt. **9**, 73 (1995).

[8] S. H. Wemple and M. DiDomenico, Appl. Solid State Sci. **3**, 263 (1972).

[9] J. Fousek, in *Proceedings of International School on Material Science and Technology*, Erice, Italia, 1986, edited by P. Günter (Springer, Berlin, 1986).

[10] U. Meier, M. Bösch, Ch. Bosshard, F. Pan, and P. Günter, J. Appl. Phys. **83**, 3486 (1998).

[11] U. Meier, M. Bösch, Ch. Bosshard, and P. Günter, Synth. Met. **109**, 19 (2000).

[12] G. Turrell, *Infrared and Raman Spectra of Crystals* (Academic Press, London, 1972).

[13] M. Walther, K. Jensby, S. R. Keiding, H. Takahashi, and H. Ito, Opt. Lett. **25**, 911 (2000).

[14] G. Knöpfle, R. Schlesser, R. Ducret, and P. Günter, Nonlinear Opt. **9**, 143 (1995).

[15] N. B. Colthup, L. H. Daly, and S. E. Wiberley, *Introduction to Infrared and Raman Spectroscopy* (Academic Press, New York, 1990).

[16] CERIUS2, Molecular Simulation (MSI), 1998.

[17] S. L. Mayo, B. D. Olafson, and W. A. Goddard, J. Chem. Phys. **94**, 8897 (1990).